J Solid State Electrochem (1998) 2: 321–327

ORIGINAL PAPER

Petr Krtil · Masahiro Yoshimura

Electrochemical preparation of oxide materials for electrochemistry and electronics

Received: 2 October 1997 / Accepted: 4 December 1997

Abstract Electrochemical formation of barium tungstate ($BaWO_4$) was studied as a model case of electrochemical formation of an advanced oxide material for electronics. $BaWO_4$ is formed on the surface of tungsten electrode during oxidation in alkaline media (pH > 12) containing a corresponding cation. The analysis of electrochemical as well as electrochemical quartz crystal microbalance (EQCM) data taken during these experiments identifies at least three qualitatively different steps composing the electrode process. Effects of the potential, applied current density and alkaline earth metal cation concentration are demonstrated using cyclic voltammetry and galvanostatic experiments. Specific constraints of the ECC formalism for the electrochemical oxide deposition following from the galvanostatic data are discussed.

Introduction

Advanced oxide materials play an important role in modern electronics as well as in electrochemistry. They make indispensable materials for applications as different as, e.g. ferroelectrics [1], light harvesting electrodes [2], electrodes for rechargeable batteries [3], etc. Despite the diversity of methods, there are two experimental approaches to preparing oxide materials for such applications. The first approach consists of a separate synthesis of the oxide [or its precursor(s)] followed by its deposition on a destination place. The other synthetic approach, which is subject of this paper, employs electrochemical deposition of an oxide (double oxide) at a surface of a conducting substrate directly in situ [4–7]. The in situ character of this preparation along with the other features, e.g. versatile control of the material's properties (film thickness, crystal size) via electrochemistry and the single-step character of the process are some of the merits of this synthetic approach.

Although the latter approach has been intensively explored [4–9], relatively little is known about the detailed mechanism of these processes, and the experimental conditions are optimized usually by a trial and error method. From the electrochemical point of view, synthetic methods described in [4–9] can be generally viewed as electrode processes proceeding by an EC (or in some cases by an ECC) mechanism, where the product of the electrochemical step is involved either in a hydrolysis [4, 7] or in a precipitation process [5, 8, 9]. Despite the differences, these two types of process can be described using similar formalism and can be controlled in a similar way.

In this paper we present the results of an electrochemical and an EQCM approach to studying the formation mechanism of oxide layers at the electrode surface. This combined approach is capable of separating and identifying different stages of the whole electrode process. Barium tungstate, formed by anodic oxidation of tungsten in alkaline media containing Ba^{2+} cation [8, 9] was chosen as a model system. A comparison of data obtained in the presence of an alkali earth metal cation (tungstate film formation) with those obtained in its absence (no tungstate film formation) was used to rationalize the relationships between the fundamental steps composing the electrode process. The electrochemical and electrochemical quartz crystal microbalance (EQCM) data also form a basis for a generalized qualitative model of the film formation.

P. Krtil[1] · M. Yoshimura (✉)
Center for Materials Design, Tokyo Institute of Technology, 4259 Nagatsuta, Midori, 226 Yokohama, Japan

Permanent address:
[1]J. Heyrovský Institute of Physical Chemistry, Academy of Sciences of the Czech Republic, Dolejškova 3, 182 23 Prague, Czech Republic

Experimental

All experiments were carried out in a three-electrode arrangement with a Pt auxiliary electrode in a home-made PTFE one-compartment cell. All potentials were measured and are quoted with respect to an Ag/AgCl reference electrode. AT-cut 9-MHz quartz crystals (International Crystal Manufacturing Company, Okla., USA) with tungsten contacts (ca. 200-nm thick, electrode area 0.25 cm^2) sputtered directly on the sides of the crystals were used as working electrodes in EQCM experiments. Electrochemical characteristics of the system were recorded using a PAR 273 potentiostat. A Seiko EG&G Quartz Crystal Analyzer QCA917 unit was used to monitor the electrode mass. Measurements were carried out in a solution containing 0.01 mol/l $Ba(OH)_2$ (analytical grade, Kanto Chemicals, Japan) and 0.1 mol/l of $NaClO_4$ (analytical grade, Wako Chemicals, Japan) as a supporting electrolyte. For experiments in Li^+-containing solution, LiOH (Wako Chemicals, Japan) in the same concentration was used instead of $Ba(OH)_2$. All solutions were prepared using Millipore Milli Q quality water, which was purged with Ar for 1 h to remove dissolved CO_2 and oxygen. The electrolyte solutions were kept under Ar prior to use. X-ray diffraction measurements were performed on an MAC Science MXP-3VA diffractometer using CuK_α radiation.

Results and discussion

Cyclic voltammetry

Cyclic voltammograms and corresponding mass change curves of a tungsten electrode in solutions containing 0.1 M $NaClO_4$ and 0.01 M LiOH and $Ba(OH)_2$ are plotted in Figs. 1 and 3, respectively.

Li^+-containing solution

In the cyclic voltammogram measured in solution containing Li^+ we can distinguish two fully pronounced anodic peaks at ca. −206 mV and 520 mV, and a shoulder at ca. 120 mV. There are no peaks during the cathodic sweep. The electrode mass change recorded simultaneously with the cyclic voltammogram brings additional information about the anodic process. In the anodic half-cycle the electrode mass remains constant until the onset of the first anodic peak and then starts to decrease. The mass decrease slows down when the potential reaches ca. 50 mV, where a plateau appears. Between 400 and 700 mV there is another mass decrease, which is finally followed by a slight mass increase at potentials positive to 800 mV. In the subsequent cathodic half-cycle, the mass signal tracks the anodic branch at first and at potentials below 800 mV another mass decrease starts, and this continues for the rest of the cycle. This very complex behavior is in accordance with previously published data on anodic behavior of W [10–13]. In detail it was described by Kelsey as a consequence of six fundamental steps:

$$W(s) + 2\,OH^- \rightarrow WO^+(s) + 3\,e^- + H_2O \quad (1)$$

$$WO^+(s) + 2\,OH^- \rightarrow WO_2(s) + e^- + H_2O \quad (2)$$

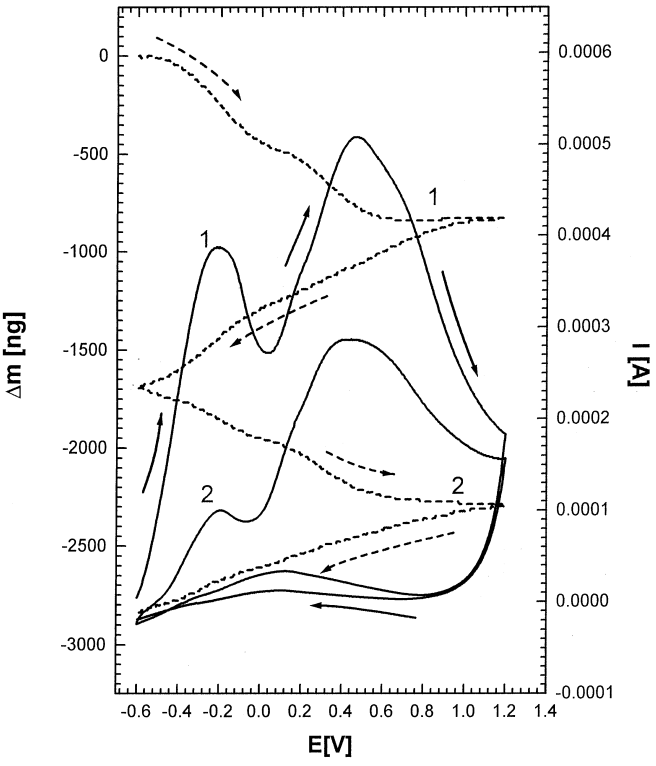

Fig. 1 Cyclic voltammogram (*solid line*) and Δm vs E (*dashed line*) curve of a tungsten electrode in 0.1 M $NaClO_4$, 0.01 M LiOH solution. Scan rate 100 mV/s

$$WO_2(s) + OH^- \rightarrow WO_3H(s) + e^- \quad (3)$$

$$WO_3H(s) + OH^- \rightarrow WO_3(s) + e^- + H_2O \quad (4)$$

$$WO_3(s) + OH^- \rightarrow HWO_4^-(aq) \quad (5)$$

$$HWO_4^-(aq) + OH^- \rightarrow WO_4^-(aq) + H_2O \quad (6)$$

The processes described by Eqs. 1–4 are electrochemical (formation of oxides at the electrode surface), and the two remaining are of a chemical character (dissolution of the oxides, eventually forming tungstate anions). The only process which can lead to a decrease of the electrode mass is the dissolution of WO_3 [14]. Therefore we can expect that already the most negative oxidation peak represents the whole six-electron oxidation process. Since there is only a little chance of separating the contribution of each of the processes 1–4 on the time-scale of our experiment, we can simplify the whole six-equation scheme by summarizing Eqs. 1–4 (i.e. those describing the reaction in which the charge is transferred) and Eqs. 5 and 6 which are of chemical nature. In such a case we obtain

$$W(s) + 6\,OH^-(aq.) \rightarrow WO_3(s) + 3H_2O + 6\,e^- \quad (7)$$

$$WO_3(s) + 2\,OH^- \rightarrow WO_4^{2-} + H_2O \quad (8)$$

After this simplification we can view the whole electrode process as a consequence of an electrochemical and a chemical step (EC sequence). The electrochemical step

(oxidation of tungsten to tungsten trioxide) and subsequent chemical step (dissolution of WO_3 in the form of WO_4^{2-}) proceed with different kinetics (depending e.g. on pH or, in the case of CV experiments, on scan rate). It can be demonstrated by the Δm vs Q curves for the beginning of the anodic scan of the first cycle at "virgin" electrode (see Fig. 2). Theoretically, if the kinetics of the dissolution is faster than that of oxide formation, then this dependence should yield a straight line with slope equal to ca. 248 g/mol. As is shown in Fig. 2, even though the slope of the Δm vs Q curve increases with decreasing scan rate it never reaches the limiting value. The presence of a plateau in the Δm vs E curves then indicates a region where the rate of oxide layer formation is equal to the rate of its dissolution. The mass behavior at potentials positive to 800 mV indicates faster formation than dissolution of an oxide. This is also confirmed by the fact that though the charge which passes through the system during the cathodic scan is negligible with respect to total charge, the total mass change during the cathodic scan represents about 40% of the total mass change. Therefore this mass signal transient should be accounted for by the dissolution of previously accumulated oxide from the electrode surface. Unfortunately, even the EQCM approach does not provide enough information to decide conclusively about the origin of the shoulder at 120 mV and the peak at 520 mV. Nevertheless, a possible explanation can be proposed based on the fact that in the experiment the electrode was oxidized in unbuffered solution. Therefore, one may anticipate a significant decrease of the pH in the close vicinity of the electrode. This causes the accumulation of the tungsten trioxide at the electrode surface. Besides this, the depletion of OH^- also influences the further oxidation process, when either OH^- or O^{2-} are transported through the surface oxide layer to the tungsten bulk. In consequence, this means that the resulting surface layer is a complex oxide material, where a significant part of the tungsten exists in an oxidation state lower than VI – probably IV or V. These oxides are then re-oxidized at more positive potentials (shoulder at 120 mV and peak at 580 mV) to WO_3. The dissolution of the eventually formed tungsten trioxide remains, however, slow. Unfortunately this hypothesis still has to be proven experimentally. An attempt to identify the composition of the oxide layer, which was formed at high potentials, by means of X-ray diffraction was unsuccessful since the presence of any other crystalline phase except that of tungsten was not confirmed.

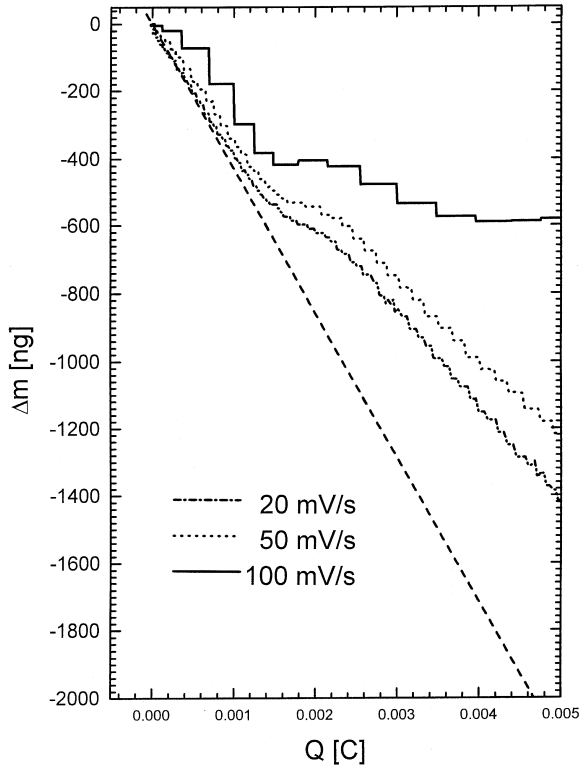

Fig. 2 Δm vs Q curves of a tungsten electrode extracted from cyclic voltammograms measured in 0.1 M $NaClO_4$, 0.01 M LiOH solution at different scan rates. *Dashed line* represents a theoretical mass response of the W dissolution. Presented charge corresponds to the potential range between initial potential (−600 mV) and 625 mV for 100 mV/s, 177 mV for 50 mV/s and 40 mV for 20 mV/s

Ba^{2+}-containing solution

In contrast to the behavior observed in Li^+-containing solutions, the voltammograms taken in Ba^{2+}-containing

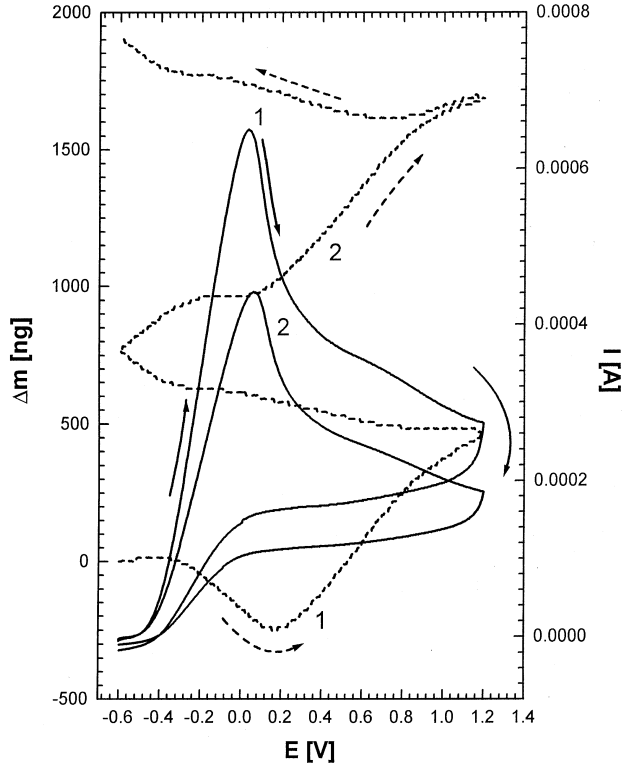

Fig. 3 Cyclic voltammogram (*solid line*) and Δm vs E (*dashed line*) curve of a tungsten electrode in 0.1 M $NaClO_4$, 0.01 M $Ba(OH)_2$ solution. Scan rate 100 mV/s

solutions (see Fig. 3) show only one anodic peak located at ca. 20 mV. An even more evident difference in the electrode process follows from the Δm vs E curve. While in the case of the Li^+-containing solution we observe a decrease in the current passing through the system, a relative increase of the peak at 520 mV comparing with that at −206 mV and no qualitative change in the Δm vs E curve in the subsequent cycle, in the Ba^{2+}-containing solutions the cyclic voltammogram does not change qualitatively in subsequent cycling, but the Δm vs E curve of the first cycle on the "virgin" electrode differs from that observed in the second cycle. During the anodic scan of the first cycle the electrode mass initially increases, then decreases and finally increases again. None of the points, where we observed the change of the Δm behavior can be linked to onset or peak potential of the current signal. During the cathodic scan we observed monotonous mass increase. Conversely, during the subsequent cycle we observed different behavior. In the electrode mass decrease during the anodic scan there is only a plateau; on the other hand during the cathodic scan the electrode mass increase is preceded by a small mass decrease at potentials negative to 1200 mV. This rather confusing behavior can be rationalized by a minor modification of the mechanism proposed for the anodic behavior of the tungsten electrode in [13]. While the processes proceeding in the absence of a film-forming cation are summarized by Eqs. 1–6, or in a simplified way by Eqs. 7 and 8 in the presence of Ba^{2+} (which acts as the film-forming cation), we should complement the reaction scheme by the following process:

$$Ba^{2+}(aq) + WO_4^{2-}(aq) \rightarrow BaWO_4(s) \quad (9)$$

We may assume that the total electrode process in the presence of Ba^{2+} is a consequence of processes 7, 8 and 9. In this way the total mass change signal combines contributions of all these processes, where the processes 7 and 9 should lead to an increase of the electrode mass, while the process 8 causes a mass decrease. Therefore the electrode mass decrease observed in the first cycle can be identified as a temporary prevailing of the contribution of the process 8 over the contributions of processes 7 and 9. Once the potential in the first cycle exceeds 300 mV, the combined contributions of processes 7 and 9 start to prevail, and this continues for the rest of the first cycle. This is true also for the rest of the experiment except for the beginning of the cathodic scan in the second cycle, when the dissolution again temporarily prevails. Since the formation of the oxide layer itself cannot be responsible for such a remarkable mass increase (compare Fig. 1), we may expect that this mass change as well as the mass increase during the cathodic scan should be accounted for by the contribution of the chemical process described by Eq. 9. It also shows that, besides the formation of the tungstate, a certain amount of oxide is still accumulated. As in the case discussed in the previous paragraph, direct evidence of this oxide layer is, however, lacking. The XRD does not reveal any other crystalline phases than $BaWO_4$ and tungsten.

A simplification of the whole process can be expected upon a change of the electrochemical perturbation. As follows from Tafel plots (see Fig. 4), the electrode process is controlled by the electrochemical step at potentials negative to 50 mV. Under such conditions we may simplify the whole mechanism by considering processes 7 and 8 as one step. Consequently the description of the mechanism of the electrode process in the presence of Ba^{2+} would apparently change from an ECC (7, 8, 9) sequence to an EC ((7 + 8), 9) sequence.

Galvanostatic experiments

Galvanostatic oxidation of W electrode at low current densities can provide the data corresponding to the requirements expressed in the previous paragraph. A comparison of the Δm vs time curves for the galvanostatic oxidation of W electrode in solutions containing Li^+ and Ba^{2+} is shown in Fig. 5. While the mass change of the electrode in Li^+-containing solutions decreases linearly with time as we may expect according to the assumption described above, in Ba^{2+}-containing solution the mass change shows more complex behavior. At first the electrode mass decreases, then passes through a minimum and then starts to increase (see Figs. 5 and 6). The time corresponding to the mass minimum t_{min} as well as total mass loss at the minimum decrease with increasing current density (see Fig. 6a). Nevertheless, a linear dependence exists between the slope of the in-

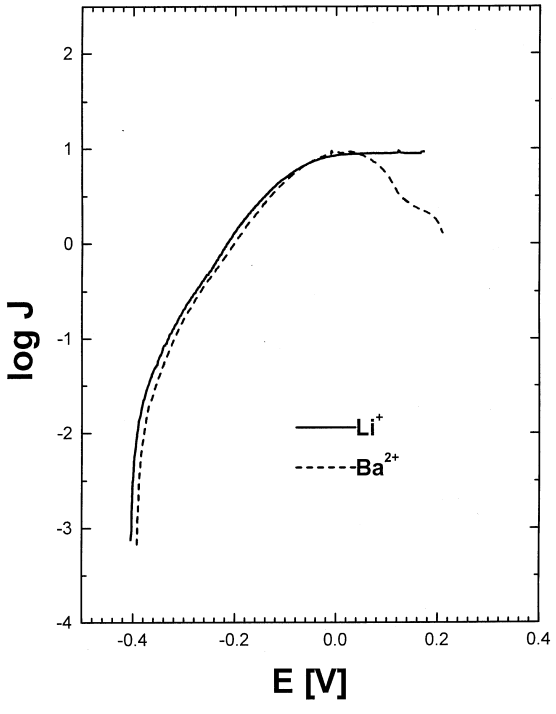

Fig. 4 Tafel plots of a tungsten electrode measured in 0.1 M $NaClO_4$, 0.01 M LiOH solution (*full curve*) and in 0.1 M $NaClO_4$, 0.01 M $Ba(OH)_2$ solution (*dashed curve*)

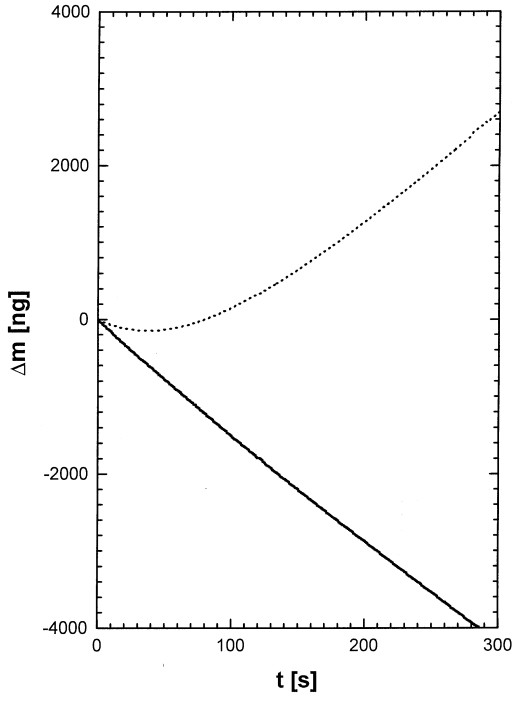

Fig. 5 Δm vs time curves taken in 0.1 M $NaClO_4$, 0.01 M LiOH solution (*full curve*) and 0.1 M $NaClO_4$, 0.01 M $Ba(OH)_2$ solution (*dotted curve*) during a galvanostatic oxidation of a tungsten electrode at 120 μAcm^{-2}

creasing part of the Δm vs time curve and current density (Fig. 6b).

At the beginning of the experiment the observed mass change tracks the mass change one would expect for simple dissolution of the tungsten electrode (see Fig. 7). This quantitative agreement indicates that there is no formation of tungstate film at the electrode at this time. The duration of this initial period depends on the applied current. The apparent molar mass extracted from the part of the Δm vs time curve, where electrode mass increases, is practically independent of current density and averages at 200 ± 8 g/mol. This value is close to what one might expect according to the combined Equations 7–9 (201 g/mol), so one might assume that under these conditions almost complete conversion of oxidized tungsten to barium tungstate occurs.

Model formulation

Driving force

The galvanostatic mass change data can be used to describe the overall kinetics of the $BaWO_4$ film formation. The simplest way is to monitor the change in the concentrations of both reactants (Ba^{2+} and WO_4^{2-}) in the vicinity of the electrode. A population of each reactant can be conveniently derived from the Nernst-Planck equation:

$$\vec{J}_j = D\nabla C_j + \frac{zF}{RT} Dc_j \nabla j\phi + c_j\vec{v} \qquad (10)$$

where c_j denotes the concentration of the reactant, D is the diffusion coefficient, ϕ is the electric potential, $\vec{v}$ is

Fig. 6 **a** Δm vs time curves of a tungsten electrode taken in 0.1 M $NaClO_4$, 0.01 M $Ba(OH)_2$ solution during galvanostatic oxidation at various current densities. **b** The $\delta(\Delta m)/\delta t$ for the increasing part of the Δm vs t curves as a function of the applied current density

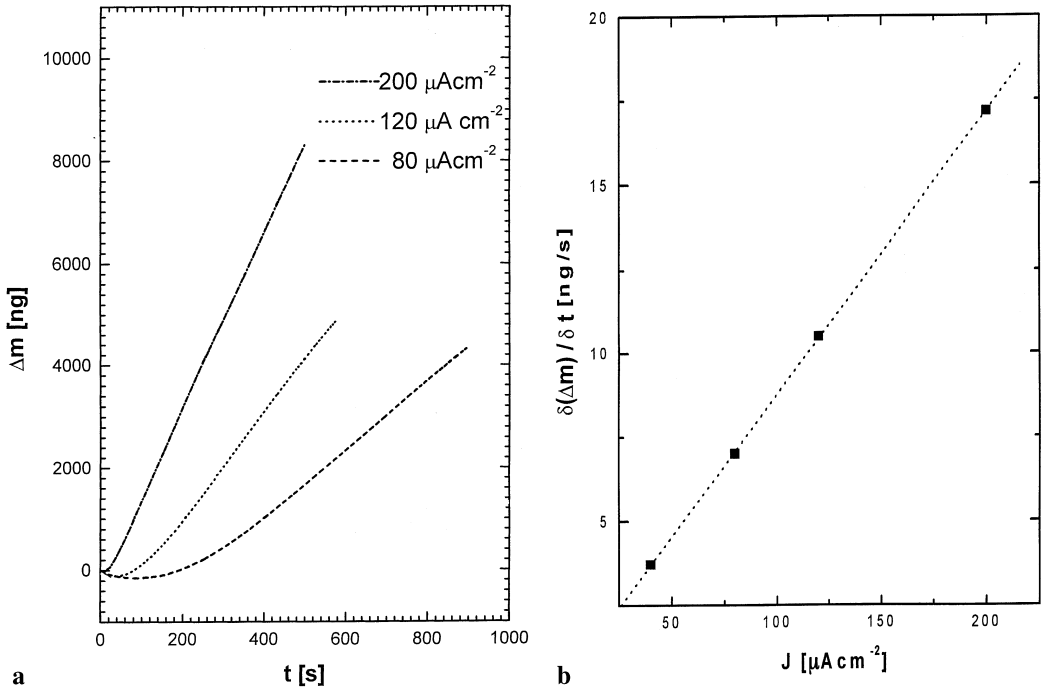

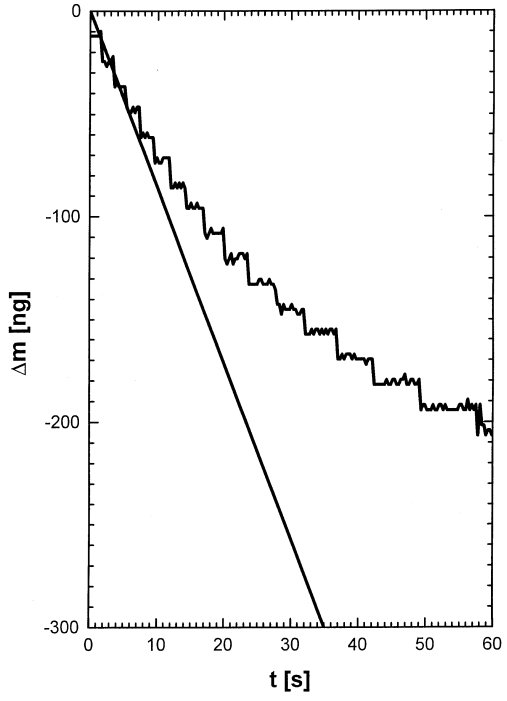

Fig. 7 A comparison of the actual Δm vs time signal for the galvanostatic formation of $BaWO_4$ with the theoretical Δm vs time signal for galvanostatic dissolution of tungsten (*straight line*); current density 80 μAcm^{-2}

the velocity of convection. The Nernst-Planck equation, however, has to be corrected for the consumption of the reactants in the chemical processes.

Though the Nernst-Planck equations for the distribution of tungstate anions and barium cations in the system are formally the same, they lead to different solutions because of the different initial and border conditions. While in the case of Ba^{2+} the initial concentration is constant and the same in the whole volume the initial concentration of tungstate anions is space-dependent and is given by the rate of the electrochemical production and subsequent distribution via such transport mechanisms as diffusion, migration and convection. If the tungstate formation is considered as a homogeneous chemical reaction, one would expect that the overall mass change observed during galvanostatic experiments should be affected by the formation of tungstate even on a very short time-scale. This is not, however, true. A more correct description can be obtained using the formalism derived to describe crystallization.

While the reaction rate of a homogeneous chemical reaction is proportional to the concentration of the reactants, the rate of crystallization is proportional to the so-called supersaturation ratio α. Supersaturation ratio is defined by the following equation

$$\alpha = \frac{a}{a^*} \tag{11}$$

where a and a^* are actual and equilibrium activities of the solute (in this case of the barium tungstate) respectively. The driving force of the process is then defined as

$$\Delta G = -RT \ln(\alpha) \tag{12}$$

where ΔG, R and T represent the change of Gibbs free energy, the universal gas constant and temperature respectively. From this definition it follows that no tungstate formation may take place unless $\alpha > 1$. In reality, however, precipitation may be still negligible even if $\alpha > 1$ but smaller than some critical value α_{cr}. A nucleation period in the process is therefore responsible, e.g. for the temporary mass decrease (due to the prevailing of the process 8) during the first cycle in Ba^{2+}-containing solution (see Fig. 3) or the initial mass decrease during the galvanostatic experiments (see Fig. 6a). Substituting the concentration with supersaturation, we may finally obtain an equation describing the time and space dependence of WO_4^{2-} and Ba^{2+} concentrations:

$$\frac{\partial c_j(x,y,z)}{\partial t} = D\nabla^2 c_j + \frac{zF}{RT} D c_j \nabla^2\phi + \bar{v}\nabla c_j - k(1-\alpha)^y \tag{13}$$

where k is a kinetic constant of precipitation. The supersaturation can be conveniently expressed using the solubility product c_s:

$$\alpha = \frac{c_{Ba^{2+}} c_{WO_4^{2-}}}{c_S} \tag{14}$$

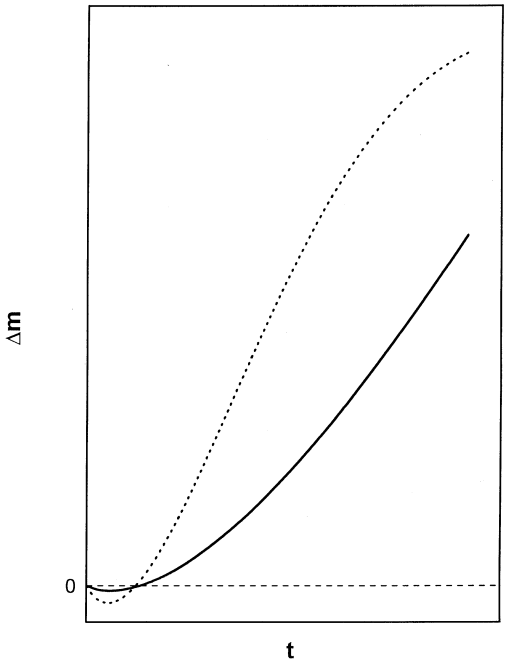

Fig. 8 Schematic representation of the Δm vs time curve for the formation of $BaWO_4$, *a* when the formation is controlled by electrochemical production of the anion (low current density *solid line*) and *b* when the film formation is controlled by the cation transport (high current density *dotted line*). The *dashed line* parallel with the *x* axis marks the electrode mass at the beginning of the galvanostatic polarization

Current density effect

As follows from the previous paragraph, the applied current density has a considerable effect on the film formation, since it controls the distribution of the tungstate anion in the system. Therefore, one may theoretically conceive of two possible regimes of the galvanostatic film deposition in dependence upon applied current density. At relatively low current density we may expect that the transport of the cation towards the electrode (given by contributions of diffusion, migration and free convection) is able to compensate for the production of the WO_4^{2-} at any time. This means that the precipitation (once the α_{cr} is achieved) occurs just in a narrow layer adjacent to the electrode surface and all the precipitate deposits as film at the electrode. Because of the electrode surface, we may expect that the nucleation is primarily heterogeneous and the critical supersaturation will be relatively low. Such behavior would produce Δm vs time curves of a similar shape to those presented in Fig. 6a. However, if the current density exceeds a certain critical value the transport of cations will not be able to compensate for the formation of tungstate anions at the electrode. Then, however, after an initial period which would resemble the previous case, the layer adjacent to the electrode would be deeply depleted of cations. Tungstate anions would be transported further to the bulk solution, which leads to a dramatic decrease in the film formation efficiency (see Fig. 8). We can anticipate that the critical current density should depend on the value of the solubility product and on the geometric arrangement as well. Detail quantitative analysis of the problem, however, has still to be done.

Acknowledgement This work was supported by the Japan Society for Promotion of Science under the contract "Research for the Future" No. 96R06901.

References

1. Burfoot JC (1967) Ferroelectrics: an introduction to the physical principles. Van Nostrand, London, p 224
2. O'Reagan B, Grätzel M (1991) Nature 353: 737
3. De Silvestro J, Haas O (1990) J. Electrochem Soc 137: 5c
4. Kavan L, O'Reagan B, Kay A, Graetzel M (1993) J Electroanal Chem 346: 291
5. Yoshimura M, Yoo S-E, Hayashi M, Ishizawa N (1989) Japan J Appl Phys 28: L2007
6. Kajiyoshi K, Tomono K, Hamaji Y, Kasanami T, Yoshimura M (1996) J Am Ceram Soc 79: 613
7. Matsumoto Y, Adachi H, Hombo J (1993) J Am Ceram Soc 73: 769
8. Cho WS, Yashima M, Kakihana M, Kudo A, Sakata T, Yoshimura M (1995) Appl Phys Lett 66: 1025
9. Cho WS, Yashima M, Kakihana M, Kudo A, Sakata T, Yoshimura M (1996) Appl Phys Lett 68: 137
10. Heumann T, Stolica N (1971) Electrochim Acta 16: 643
11. Heumann T, Stolica N (1971) Electrochim Acta 16: 1635
12. Armstrong RD, Edmundson K, Firman RE (1972) J Electroanal Chem 40: 19
13. Kelsey GS (1977) J Electrochem Soc 124: 814
14. Deltombe E, De Zoubov N, Pourbaix M (1974) Atlas of electrochemical equilibria in aqueous Solutions, tungsten section. National Association of Corrosion Engineers, Houston, USA